[12] J. L. Fikart and P. A. Goud, "A theory of oscillator noise and its application to IMPATT diodes," *J. Appl. Phys.*, vol. 44, pp. 2284–2296, 1973.
[13] M. T. Vlaardingerbroek, "Output spectrum of IMPATT-diode oscillators," *Electron. Lett.*, vol. 5, pp. 521–522, 1969; J. J. Goedbloed and M. T. Vlaardingerbroek, "On the theory of noise and injection phase locking of IMPATT-diode oscillators," *Philips Res. Rep.*, vol. 25, pp. 452–471, 1970.
[14] J. J. Goedbloed, "FM noise of low-level operating IMPATT-diode oscillators," *Electron. Lett.*, vol. 7, pp. 445–446, 1971.
[15] ——, "On the up-converted noise of IMPATT-diode oscillators," in *Proc. MOGA Conf.*, Amsterdam, 1970, pp. 12.36–12.40.
[16] J. J. Goedbloed, "Intrinsic AM noise in singly tuned IMPATT-diode oscillators," *IEEE Trans. Electron Devices*, vol. ED-20, pp. 752–754, Aug. 1973.
[17] G. Convert, "Sur la theorie du bruit des diodes à avalanche," *Rev Tech. Thomson-CSF*, vol. 3, pp. 419–471, 1971.
[18] M. E. Hines, "Large-signal noise, frequency conversion, and parametric instabilities in IMPATT-diode networks," *Proc. IEEE*, vol. 60, pp. 1534–1548, Dec. 1972.
[19] B. B. v. Iperen and H. Tjassens, "Novel and accurate methods for measuring small-signal and large-signal impedances of IMPATT-diodes," *Philips Res. Rep.*, vol. 27, pp. 38–75, 1972.
[20] J. C. Inkson, "Noise generation under large-signal conditions in the Read microwave avalanche diode," *Int. J. Electron.*, vol. 25, pp. 1–16, 1968.
[21] D. E. Iglesias, "Circuit for testing high-efficiency IMPATT-diodes," *Proc. IEEE* (Lett.), vol. 55, pp. 2065–2066, Nov. 1967.
[22] K. Kurokawa and F. M. Magelhaes, "An *X*-band 10-Watt Multiple-IMPATT Oscillator," *Proc. IEEE* (Lett.), vol. 59, pp. 102–103, Jan. 1971.
[23] J. J. Goedbloed, "Determination of the intrinsic response time of semiconductor avalanches from microwave measurements," *Solid-State Electron.*, vol. 15, pp. 635–647, 1972.
[24] A. v.d. Ziel, *Noise.* Englewood Cliffs, N. J.: Prentice-Hall, 1954, pp. 321–322.
[25] R. J. McIntyre, "Multiplication noise in uniform avalanche diodes," *IEEE. Trans. Electron Devices*, vol. ED-13, pp. 164–168, Jan. 1966.
[26] R. Zurmühl, *Matrizen.* Berlin: Springer, 1964.
[27] G. Weidmann, "Modulation of IMPATT-diode oscillators," Paper presented at ESSDERG, München, 1971.
[28] K. Mouthaan and H. P. M. Rijpert, "Nonlinearity and noise in the avalanche transit-time oscillator," *Philips Res. Rep.*, vol. 26, pp. 391–413, 1971.
[29] J. J. Goedbloed, "Noise in IMPATT-diode oscillators," Thesis, *Philips Res. Rep.* Supplements. no. 7, 1973.
[30] D. de Nobel, "IMPATT-diode technology," presented at the Avalanche Diode Workshop, New York, Dec. 1969.
[31] H. Tjassens, "Stable and low-noise IMPATT diode oscillator for *X* band," in *Proc. 1973 European Microwave Conf.*, Brussels, vol. 1, 1973, paper A.1.2.
[32] B. B. van Iperen, "Efficiency limitation by transverse instability in IMPATT diodes," *Proc. IEEE.* (Lett.), vol. 62, pp. 284–285, Feb. 1974.

Vertical Multijunction Solar-Cell One-Dimensional Analysis

AVRAHAM GOVER, STUDENT MEMBER, IEEE, AND PAUL STELLA, MEMBER, IEEE

***Abstract*—The vertical multijunction solar cell is a photovoltaic device which may allow conversion efficiencies higher than conventional planar devices. A one-dimensional model of the device is presented here which allows a simple and straightforward analysis of device performance to be conducted.**

The analysis covers the derivation of device short-circuit current, saturation current, open-circuit voltage, and maximum power as a function of illumination spectra, device geometry, and device material properties.

LIST OF SYMBOLS

n,p	Excess electrons and holes concentration (cm^{-3}).
j_n,j_p	Excess electrons and holes current density (cm^{-3}).
j_L	Pairs generation rate at depth z ($cm^{-3}\ s^{-1}$).
τ_n,τ_p	Excess electron and hole lifetime (s).
D_n,D_p	Electron and hole diffusion constants (cm^2/s).
L_n,L_p	Electron and hole diffusion lengths (cm).
N_A,N_D	Acceptor and donor impurity concentrations (cm^{-3}).
$I_{SR}(\lambda)$	Spectral response; defined as the output current for one unit of input power at wavelength λ (A/W).
I_{sc}	Short-circuit current (A).
V_0	Open-circuit current (V).
$N(\lambda)$	Photon flux density ($cm^{-2}\ s^{-1}$).
$\alpha(\lambda)$	Absorption coefficient of the cell material [5] (cm^{-1}).
η_a	Absorption efficiency; defined as the fraction of impinging light which is absorbed by the cell.
η_{coll}	Collection efficiency; defined as the fraction of generated pairs which is collected by the junctions.
γ	Conversion efficiency; defined as the maximum-output electrical power fraction of the input power.
P_{in}	Input radiation power density (W/cm^2).
W_1,W_2	p- and n-region widths (cm).
h	Cell thickness (cm).
N_0	Air-mass zero solar photon flux density (3.45×10^{17} photons/$cm^2 \cdot s$). The cell y-dimension width is assumed to be 1 cm.

Manuscript received January 22, 1973; revised December 12, 1973. This work was conducted under Air Force Contract F33615-72-C-1310.
The authors are with Heliotek, Sylmar, Calif. 91342.

I. INTRODUCTION

THE vertical junction solar cell, shown schematically in Fig. 1, is potentially a more efficient device compared to the conventional planar cell. The advantage results mainly from the possibility of using highly doped p and n regions to provide high voltage factors, without incurring severe reduction in the generated carrier collection efficiency, and without requiring advances in material properties.

Although junction voltage improvement can be obtained with the conventional planar cell by using high impurity concentration material, there is very little which can be done to prevent a pronounced reduction of the collection efficiency due to the reduction of the excess carrier diffusion length. This loss can become severe enough to cancel the improvement gained in the junction voltage. In comparison, this loss can be avoided in the vertical junction cell by reducing the distance between the junctions so that it is smaller than the reduced diffusion length. The intent of this paper is to investigate the vertical junction cell parameters and to present them in a useful model which will allow for simple calculation of the cell performance.

In our model, the following assumptions have been made for simplicity: zero front- and rear-surface recombination velocities, homogeneous n and p regions, no front-surface reflection losses, and no ohmic losses. Furthermore, the carrier recombination process in the junction space-charge region is neglected.

II. COLLECTION EFFICIENCY AND SHORT-CIRCUIT CURRENT

Although the carrier generation rate is z dependent (see Fig. 1(a)), the assumption of zero surface recombination allows us to consider only the one-dimensional problem of excess carrier current flow in the x direction. This will allow for simple analytical solutions and expressions for the cell parameters.

Looking first at p-type material, the minority carrier diffusion current in the x direction at some fixed depth z is (see Fig. 1(a)) [1]

$$j_n = qD_n \frac{\delta n(x)}{\delta x}. \tag{1}$$

The continuity equation is then

$$\frac{1}{q}\frac{\delta j_n}{\delta x} - \frac{n(x)}{\tau_n} = -j_L. \tag{2}$$

For monochromatic illumination of wavelength λ, the equation is

$$j_L = \alpha(\lambda) N(\lambda) \exp(-\alpha z). \tag{3}$$

Equations (1) and (2) are then combined to yield

$$L_n^2 \frac{\delta^2 n(x)}{\delta x^2} - n(x) = -\tau_n j_L \tag{4}$$

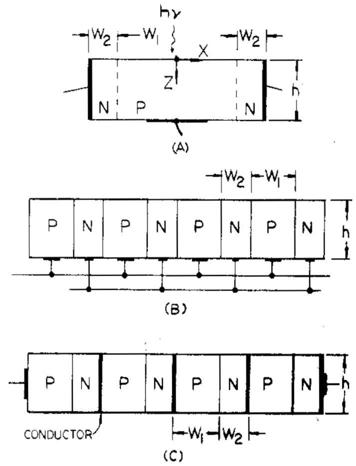

Fig. 1. Vertical junction cell configurations.

where

$$L_n = (D_n \tau_n)^{1/2}. \tag{5}$$

At the junctions, the short-circuit condition determines the excess minority carrier boundary values (using the cell center line as the origin) as

$$n\left(-\frac{W_1}{2}\right) = n\left(\frac{W_1}{2}\right) = 0. \tag{6}$$

The solution of (4) with (6) is, for any fixed z,

$$n(x) = \tau_n j_L(z)\left[1 - \frac{\cosh x/L_n}{\cosh W_1/2L_n}\right]. \tag{7}$$

This distribution is illustrated in Fig. 2.

The generated current, which is collected per unit length at depth z from the surface in each junction, is

$$j_n(z) = -qD_n \left.\frac{\delta n}{\delta x}\right|_{x=W_1/2} = qL_n j_L \tanh \frac{W_1}{2L_n}. \tag{8}$$

For an n-type region, the same results apply with the subscript p substituted for n and W_2 substituted for W_1.

The solution of the differential equation is valid for any of the homogeneous n- or p-type regions in each of the configurations presented in Fig. 1, since (6) applies both at a junction or at an ohmic contact. The difference is that the electron-hole pairs arriving at the junction separate and contribute useful current, while pairs arriving at the ohmic contact recombine and do not contribute any externally useful current.

Considering 1(a), the total current collected per unit length at depth z is

$$j(z) = 2qj_L(z)\left[L_n \tanh \frac{W_1}{2L_n} + L_p \tanh \frac{W_2}{2L_p}\right]. \tag{9}$$

We define the function η_c (plotted in Fig. 3) as

$$\eta_c(u) = \frac{1}{u}\tanh u \tag{10}$$

and call $\eta_{c1} = \eta_c(W_1/2L_n)$ and $\eta_{c2} = \eta_c(W_2/2L_p)$ the col-

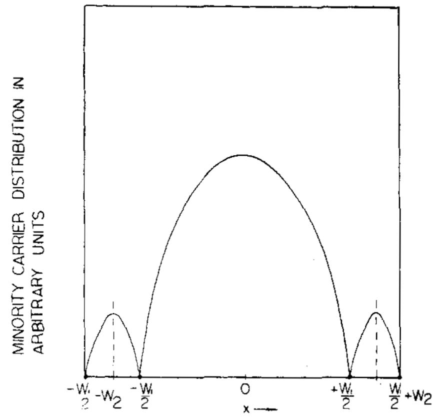

Fig. 2. Minority carrier distribution for the configuration of Fig. 1(a).

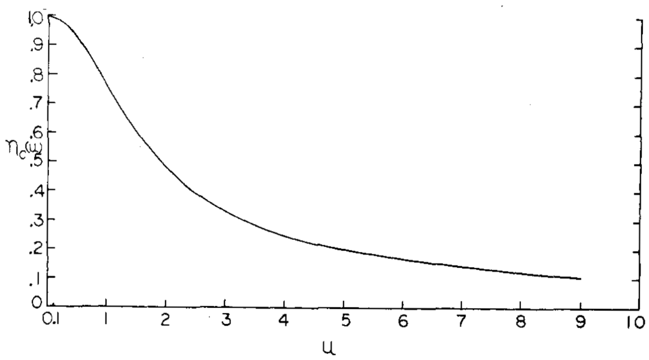

Fig. 3. Collection efficiency (η_c).

lection efficiency factors for the p and n regions, respectively. Then,

$$j(z) = qj_L(z)[W_1\eta_{c1} + W_2\eta_{c2}]. \tag{11}$$

The total current collected in the cell is obtained by integrating over z. Integrating (11), using (3) for $j_L(z)$, we obtain the expression for the short-circuit current collected by the cell when illuminated by light of wavelength λ, as seen by

$$I_{sc}(\lambda) = qN(\lambda)[1 - \exp[-\alpha(\lambda)h]](W_1\eta_{c1} + W_2\eta_{c2}). \tag{12}$$

Using the definitions of absorption efficiency, η_a, and collection efficiency, η_{coll}, we find

$$\eta_a = 1 - \exp(-\alpha h) \tag{13}$$

$$\eta_{coll} = \frac{I_{sc}(\lambda)}{q\eta_a N(\lambda)(W_1 + 2W_2)} = \left[\frac{W_1\eta_{c1} + W_2\eta_{c2}}{W_1 + 2W_2}\right]. \tag{14}$$

The short-circuit current can be rewritten as

$$I_{sc}(\lambda) = q\eta_a\eta_{coll}(W_1 + 2W_2)N(\lambda). \tag{15}$$

Interestingly, the collection efficiency of the vertical junction cell is found to be independent of wavelength, in contrast to the planar cell. This is due to the fact that the depth at which radiation is absorbed (a wavelength-dependent function) does not change the junction-to-carrier distance. In the conventional planar cell, the junction-to-carrier distance varies with the absorption depth.

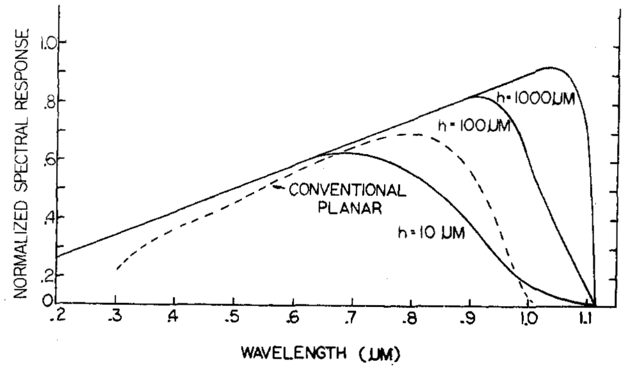

Fig. 4. Vertical junction cell spectral response.

The spectral response of the cell is by definition,

$$I_{SR}(\lambda) = \frac{I_{sc}(\lambda)}{(W_1 + 2W_2)P_{in}}. \tag{16}$$

Substituting in (15), we find

$$N(\lambda) = \frac{P_{in}(\lambda)}{hc/\lambda} \tag{17}$$

and using in (16), we get

$$I_{SR} = \frac{q\lambda}{hc}\eta_{coll}\eta_a. \tag{18}$$

The spectral response of the vertical cell is plotted in Fig. 4 for various values of thickness (h). In comparison to the planar cell, the vertical solar-cell spectral response is better in both the long and short wavelengths, and it tends to the ideal response shape for large values of h.

All the expressions derived in the preceeding have been calculated for the cell configuration of Fig. 1(a). However, it is quite easy to modify them to the other configurations. For the cell 1(b), the collection efficiency is written as

$$\eta_{coll} = \frac{W_1\eta_{c1} + W_2\eta_{c2}}{W_1 + W_2} \tag{19}$$

and the short-circuit current as

$$\begin{aligned} I_{sc}(\lambda) &= q\eta_a\eta_{coll}m\left(\frac{W_1 + W_2}{2}\right)N(\lambda) \\ &= \frac{m}{2}qN(\lambda)(1 - \exp[-\alpha h])(W_1\eta_{c1} + W_2\eta_{c2}) \end{aligned} \tag{20}$$

where m is the number of junctions in the cell. The spectral response is still described in (18) and Fig. 4, but η_{coll} in that equation is given by (19). Since all the excess carrier pairs which arrive at the ohmic contacts recombine and do not contribute external current, the generated current collected in the cell configuration 1(c) is essentially half the current collected by the cell 1(b). Therefore, its collection efficiency, the short-circuit current, and the spectral response will be exactly half of (19), (20), and (18), respectively.

Normally we desire to know the cell's performance relative to some given light spectrum $N(\lambda)$. This can be accomplished by integrating either (12) or (20) over all wavelengths λ shorter than the bandgap wavelength λ_0. In the numerical calculation which follows, we use the air-mass zero solar spectrum reported by Thekakara [2], and assume for silicon $\lambda_0 = 1.1\ \mu$. Hence, we get

$$I_{sc} = \int_0^{\lambda_0} I_{sc}(\lambda)\, d\lambda. \tag{21}$$

Let

$$N_0 = \int_0^{\lambda_0} N(\lambda)\, d\lambda. \tag{22}$$

Then,

$$\eta_A = \frac{1}{N_0} \int_0^{\lambda_0} N(\lambda)\,(1 - \exp[-\alpha(\lambda)h])\, d\lambda \tag{23}$$

is defined as the polychromatic absorption efficiency. N_0 is the maximum number of photons in the spectrum that may be absorbed by band-to-band transition. It is therefore a characteristic number for the given spectrum relative to the given semiconductor.

Using this definition, we interpret the absorption efficiency for the polychromatic spectrum to be the fraction of N_0 photons absorbed in the cell rather than to be the fraction of the total number of incident photons, so that $0 \leq \eta_A \leq 1$. Then, using (21) and (23), the short-circuit current for case 1(a) is

$$I_{sc} = (W_1 + 2W_2)\eta_{coll}\eta_A q N_0 \tag{24}$$

and in case 1(b), it is

$$I_{sc} = \frac{m}{2}(W_1 + W_2)\eta_{coll}\eta_A q N_0. \tag{25}$$

The collection efficiency η_{coll}, being independent of wavelength, is the same as in the monochromatic illumination case, and is given by (14) or (19). The absorption efficiency, η_A, for air-mass zero spectrum is given in Fig. 5 for various values of cell thickness (h), where the parameter N_0 calculated from (22) is

$$N_0 = 3.45 \times 10^{17}\ \text{photons/cm}^2\cdot\text{s}.$$

III. CURRENT–VOLTAGE CHARACTERISTICS AND CONVERSION EFFICIENCY

If we now allow a voltage across the junctions, (4) is still valid, but (6) must be changed to

$$n\left(\pm \frac{W_1}{2}\right) = n_p\left(\exp\left[\frac{qV}{kT}\right] - 1\right) \equiv n_1 \tag{26}$$

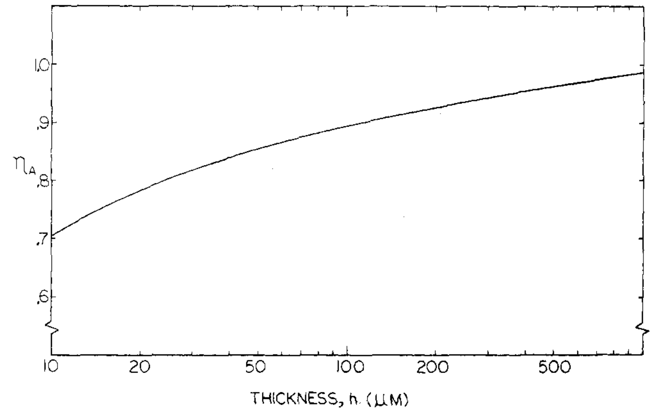

Fig. 5. Absorption efficiency (η_A) versus cell thickness.

for the p-type region, and

$$p\left(\pm \frac{W_2}{2}\right) = p_n\left(\exp\left[\frac{qV}{kT}\right] - 1\right) \equiv p_1 \tag{27}$$

for the n region where

$$n_p = \frac{n_i^2}{n_A}, \qquad p_n = \frac{n_i^2}{n_D}. \tag{28}$$

The solution of the differential equation with these boundary conditions is (for p region)

$$n(x) = [n_1 - \tau_n j_L(z)]\frac{\cosh x/L_n}{\cosh W_1/2L_n} + \tau_n j_L(x). \tag{29}$$

Then, for a given wavelength, the junction current density at depth z from the surface is

$$\begin{aligned} j_n(z) &= -qD_n \left.\frac{\delta n}{\delta x}\right|_{x=W_1} \\ &= [\tau_n j_L(\lambda,z) - n_1]\frac{qD_n \tanh(W_1/2L_n)}{L_n}. \end{aligned} \tag{30}$$

In a similar fashion, the n-region contribution to the junction current density is

$$j_p(z) = [\tau_p j_L(\lambda,z) - p_1]\frac{qD_p \tanh(W_2/2L_p)}{L_p}. \tag{31}$$

Hence, the total current density per junction is

$$\begin{aligned} j(z) &= j_n(z) + j_p(z) \\ &= qj_L(z)\left[\frac{W_1\eta_{c1}}{2} + \frac{W_2\eta_{c2}}{2}\right] - q\left[\frac{n_1W_1\eta_{c1}}{2\tau_n} + \frac{p_1W_2\eta_{c2}}{2\tau_p}\right] \end{aligned} \tag{32}$$

where we made use of (5) and (10). The total current per junction is obtained by integrating (32) over z using (3), (26), (27), and (28), as seen by

$$I = qN(\lambda)(1 - \exp[-\alpha h])\left[\frac{W_1\eta_{c1}}{2} + \frac{W_2\eta_{c2}}{2}\right]$$

$$- qn_i^2 h \left[\frac{W_1 \eta_{c1}}{2N_A \tau_n} + \frac{W_2 \eta_{c2}}{2N_D \tau_p}\right] \left(\exp\left[\frac{qV}{kT}\right] - 1\right). \quad (33)$$

Proper summation of the contributions from each junction yields, for all configurations, the dependence

$$I = I_{sc} - I_0 \left(\exp \frac{qV}{kT} - 1\right) \quad (34)$$

where, for configuration 1(a),

$$I_0 = qn_i^2 h \left[\frac{W_1 \eta_{c1}}{N_A \tau_n} + \frac{W_2 \eta_{c2}}{N_D \tau_p}\right] \quad (35)$$

with the I_{sc} given by (12) or (15), and for configuration 1(b),

$$I_0 = \frac{m}{2} qn_i^2 h \left[\frac{W_1 \eta_{c1}}{N_A \tau_n} + \frac{W_2 \eta_{c2}}{N_D \tau_p}\right] \quad (36)$$

with I_{sc} given by (20).

For polychromatic illumination, integration over λ must also be carried out. Equations (34), (35), and (36) are still valid in this case, but the expressions for I_{sc} to be used in (34) are (24) and (25) for configurations 1(a) and 1(b), respectively.

A. Open-Circuit Voltage

From (34), the open-circuit voltage is

$$V_0 = \frac{kT}{q} \ln \frac{I_{sc}}{I_0}. \quad (37)$$

Substituting (14), (24), and (35), or alternatively (19), (25), and (36), we have for configurations (a) and (b)

$$V_0 = \frac{kT}{q} \ln \left[\frac{N_0 \eta_A}{hn_i^2} (W_1 \eta_{c1} + W_2 \eta_{c2}) \bigg/ \left(\frac{W_1 \eta_{c1}}{N_A \tau_n} + \frac{W_2 \eta_{c2}}{N_D \tau_p}\right)\right]. \quad (38)$$

For 1(a) with $W_2 \ll W_1$ and $N_D \gg N_A$, the n-region contribution to both the generated current and the diode saturation current is negligible, so to a very good approximation,

$$V_0 = \frac{kT}{q} \ln \frac{\tau_n N_0 N_A \eta_A}{hn_i^2}. \quad (39)$$

For the same cell configuration, but with opposite conductivity, i.e., the base is an n type,

$$V_0 = \frac{kT}{q} \ln \frac{\tau_p N_0 N_D \eta_A}{hn_i^2}. \quad (40)$$

Observe that the open-circuit voltage is in this case independent of the cell width. This is because the collected and saturation currents both have the same functional dependence on width, thereby cancelling any width dependence from the V_{oc} expression. However, the V_{oc} is quite dependent on the cell thickness with an increasing h providing a decreasing V_{oc}.

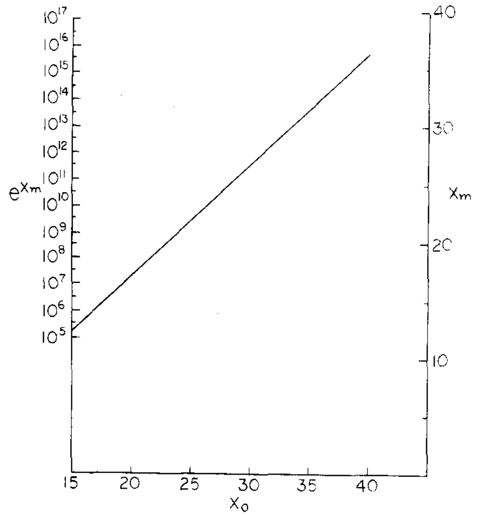

Fig. 6. Solution to (44) (maximum power condition).

B. Power Output

The maximum power available from the solar cell is obtained when

$$\frac{d}{dV}(IV) = \frac{d}{dV}\left[\left(I_{sc} - I_0 \exp\left[\frac{qV}{kT}\right]\right) V\right] = 0. \quad (41)$$

The solution of this equation is

$$V_m = \frac{kT}{q} X_m \qquad \text{(maximum power voltage)} \quad (42)$$

$$I_m = I_{sc} - I_0 \exp[X_m] \qquad \text{(maximum power current)} \quad (43)$$

where X_m is the solution of the transcendental equation

$$X + \ln(1 + X) = X_0 \quad (44)$$

and

$$X_0 = \frac{q}{kT} V_0. \quad (45)$$

Equation (44) was numerically solved for various values of X_0, and the parameter X_m is plotted as function of X_0 in Fig. 6. For a given cell structure, V_0 and X_0 may be calculated using (38) and (45) and, with the aid of Fig. 6, V_m and I_m are calculated from (42) and (43). The maximum power available from the cell is then

$$P_m = I_m V_m. \quad (46)$$

C. Conversion Efficiency

The power input into the solar cell is $P_{in}A$, where A is the cell area, and P_{in} is the radiation power density shining on the cell. For air-mass zero solar radiation [2],

$$P_{in} = 135.3 \text{ mW/cm}^2. \quad (47)$$

The conversion efficiency is given for the configuration (a) by

$$\gamma = \frac{P_m}{(W_1 + 2W_2)P_{\text{in}}} \tag{48}$$

and for configuration (b) by

$$\gamma = \frac{P_m}{(m/2)(W_1 + W_2)P_{\text{in}}}. \tag{49}$$

IV. EXAMPLES

To demonstrate the use of the model analysis and to display the numerical value of the vertical junction performance parameters, a sample calculation is shown. We chose a p-base cell of configuration 1(a), where

$$h = 100\ \mu\text{m}, \quad W_1 = 20\ \mu\text{m}, \quad N_A = 5 \times 10^{17}\ \text{cm}^{-3}.$$

From [3] and [4] for this impurity concentration, we have

$$\tau_n = 1.1\ \mu\text{s}, \quad D_n = 10\ \text{cm}^2\cdot\text{s}^{-1}, \quad L_n = 33\ \mu\text{m}.$$

If we assume $W_2 \ll W_1$, then (19) reduces into

$$\eta_{\text{coll}} = \eta_{c1} = \eta_c\left(\frac{W_1}{2L_n}\right) = 0.97$$

where Fig. 3 is used to evaluate η_c. The absorption efficiency for air-mass zero solar illumination is found from Fig. 5 and seen as

$$\eta_A = 0.89.$$

The short-circuit current and the saturation current are found from (24) and (35) and seen as

$$I_{sc} = 0.1\ \text{mA}$$

$$I_0 = 8.5 \times 10^{-13}\ \text{mA}.$$

Using (39) and (45), we have

$$X_0 = 25.5$$

$$V_0 = 662\ \text{mV}.$$

Then with the aid of Fig. 6, using (42) and (43), we have

$$X_m = 22.3$$

$$V_m = 580\ \text{mV}$$

$$I_m = 0.09\ \text{mA}.$$

The maximum power output of the cell is therefore

$$P_m = I_m V_m = 0.05\ \text{mW}$$

and the conversion efficiency is

$$\gamma = \frac{P_m}{P_{\text{in}}W} = 19.7\ \text{percent}.$$

V. CONCLUSION

The above model provides a description of vertical junction solar-cell behavior. It is proposed that such a structure can provide hitherto unobtained conversion efficiencies. Efficiencies which are predicted for ideal planar cells (with exceptional material properties and lifetimes [6]) are achievable in the vertical cell, utilizing present-day state-of-the-art material properties.

The conversion efficiency of the cell calculated in the example in the previous section exceeds the conversion efficiency of recently reported high-efficiency planar cells [7] by more than 40 percent. Yet the freedom in choosing the structural parameters may allow even higher efficiencies.

The impact of additional effects listed briefly in the introduction, but not discussed in the present paper, will reduce some of the advantages predicted by the one-dimensional model. At present, the authors are preparing an additional paper which will include an analysis of these effects and their expected impact. Of prime importance is the realization of fabrication techniques capable of providing the high junction density required for best operation. It is possible that techniques such as preferential etching and epitaxy can provide optimized structures with a few year's effort.

ACKNOWLEDGMENT

The authors wish to thank W. P. Rahilly, M. Wolf, T. Chadda, and J. Scott-Monck for their helpful comments and assitance during this program.

REFERENCES

[1] William Shockley, *Electrons and Holes in Semiconductors*. New York, N. Y.; Van Nostrand, 1950.
[2] M. P. Thekaekara, "Evaluating the light from the sun," *Opt. Spectra*, p. 32, Mar. 1972.
[3] S. M. Sze and J. C. Irvin, "Resistivity, mobility, and impurity levels in GaAs, Ge, and Si at 300°K," *Solid-State Electron.*, vol. 11, p. 599, 1968.
[4] B. Ross and J. R. Madigan, "Thermal generation of recombination centers in silicon," *Phys. Rev.*, vol. 108, no. 6, p. 1428–33, Dec. 1957.
[5] H. Y. Fan *et al.*, *Infra-Red Absorption and Energy-Bond Structure of Germanium and Silicon*, New York, N. Y.; Wiley, 1956, p. 184.
[6] M. Wolf, "A new look at silicon solar cell performance," in *8th IEEE Photovoltaic Specialists Conf.*, 1970, p. 360.
[7] J. Lindmayer and J. Allison, "An improved silicon solar cell, the violet cell," in *9th IEEE Photovoltaic Specialists Conf.*, 1972, p. 83.